J-Stage Released Online Advance Publication: February 21, 2025

Food Science and Technology Research, **31** (3), 169–183, 2025

doi: 10.3136/fstr.FSTR-D-24-00238

https://jsfst.smoosy.atlas.jp

Original Paper

Coarse-grained dynamics simulation of the grain-filled structure of rice balls

Makoto MIURA[1*], Tatsuya ISHII[2], Yuko TANAKA[3], Tomoka YANATA[3], Shin YONEYAMA[4], and Pengyu XU[4]

[1] *Collaborative Research Programs of SynCrest Inc., Faculty of Agriculture, Iwate University, 3-18-8 Ueda, Morioka, Iwate 020-8550, Japan*

[2] *Division of Agriculture, Graduate School of Arts and Sciences, Iwate University, 3-18-3 Ueda, Morioka, Iwate 020-8550, Japan*

[3] *Department of Biological Chemistry, Faculty of Agriculture, Iwate University, 3-18-8 Ueda, Morioka, Iwate 020-8550, Japan*

[4] *Head office and laboratory, SYNCREST Inc., Shonan Health Innovation Park, 2-26-1 Muraokahigashi, Fujisawa, Kanagawa 251-0012, Japan*

Received December 10, 2024 ; Accepted February 13, 2025

Rice is eaten as an aggregate of rice grains, and its perceived texture during oral processing changes with every chew. Mass production of rice balls with controllable food texture is still difficult because the relationship between the rice grain-packing structure and mechanical properties and food texture of rice balls is still unknown. This study aims to clarify the causal relationships between (1) the molding conditions of the rice ball and grain-filling structure, (2) the grain-filling structure and its texture, and (3) the mechanical properties of the rice ball and its texture. Using a rice grain-packing structure model which reflects the physical and chemical properties of the rice grains and balls in a coarse-grained dynamics simulation, changes in the packing structure during compression were observed, and the relationship between the rice grain-packing structure and mechanical properties of the rice balls was clarified. Furthermore, the behavior of rice grains during actual rice mass compression was successfully simulated using the developed rice grain-filling model. Our measurements and simulation results pave the way for an industrial method of producing rice balls with arbitrary food textures.

Keywords: rice ball, food texture, coarse-grained dynamics simulations, grain-filled structure

Introduction

The annual per capita rice consumption is 51.1 kg in 2023 and has been decreasing year by year, but the rate of decrease has slowed down in recent years[i]. In contrast, the annual production of processed rice in 2022 is 440 000 tons, and the production index is increasing year by year at 2.6 % over the previous year[ii]. Processed rice is a generic term for retort-packed rice, aseptically packaged rice, frozen rice, chilled rice, dried rice, and canned rice. Onigiri (Omusubi, Nigirimeshi) is a traditional Japanese rice dish, made of freshly cooked white rice that is hand-rolled to form a triangular or circular cross section. In some cases, rice is filled or wrapped in nori (seaweed). Nigiri-sushi is another traditional Japanese dish, made by placing thin slices of fresh fish or other ingredients on a hand-shaped small ball of rice seasoned with rice vinegar, sucrose, and salt. These rice balls for onigiri and nigiri-sushi are processed into frozen rice balls for commercial use.

In recent years, many food robots have been developed in the food industry to improve work efficiency, as presented in previous literatures (Derossi *et al*., 2023; Pan *et al*., 2024; Xu *et al*., 2024). For instance, rice processing machines have been used in conveyor-belt sushi restaurants and supermarket kitchens to improve work efficiency and reduce costs. However, ideal mechanical properties of rice balls have not been achieved yet by these machines; rice grains are firmly molded before eating, but the rice ball easily disintegrates in

*To whom correspondence should be addressed. E-mail address: mako@iwate-u.ac.jp

the mouth during chewing. Physical and chemical properties of rice grains vary depending on rice varieties and growth conditions (Li *et al*., 2023; Mengjie *et al*., 2024; Nakamura *et al*., 2016; Zhang *et al*., 2024), rice grain structure and composition (Li *et al*., 2023; Yin *et al*., 2023; Zuo *et al*., 2024), milling condition (Zhang *et al*., 2023; Zhang *et al*., 2024), storage conditions (Chen *et al*., 2024; Garofalo *et al*., 2024), milled rice pre-treatment (Liu *et al*., 2024; Tien *et al*., 2024; Panngom *et al*., 2024), cooking process, *i.e*., soaking conditions (Chen *et al*., 2024; Wu *et al*., 2023), mass ratio of milled rice to water (Tamura *et al*., 2024; Yi *et al*., 2024), and heating control. The physicochemical properties of rice balls also vary depending on the density, void volume, molding speed, and other factors (Kim *et al*., 2017). Moreover, food texture significantly contributes to the eating quality of rice (Kwak *et al*., 2015). While there have been many studies on the physicochemical characteristics of rice grains, studies are few on rice balls (Miao *et al*., 2016; Xu *et al*., 2024), which are rice grain aggregates. To prepare rice balls with good food texture, their mechanical properties must be measured, considering the interaction forces among individual rice grains of the rice ball along with the grain-packing structure within the rice ball. However, the rice grain-packing structure cannot be arbitrarily changed, and the causal relationships between the packing structure and mechanical properties and food texture of the rice ball is still unknown. The friction and free space between particles and their compressive behavior have been studied in the industry (Kim *et al*., 2024; Tong *et al*., 2024; Zheleznyakova *et al*., 2021), but studies are few in food research. Therefore, we decided to use a coarse-grained molecular dynamics simulation method in this study using rigid particles. The term "coarse-grained" is used to describe a concept that has been commonly used in statistical mechanics to describe the statistical behavior of the entire system (Chibrikov *et al*., 2024; Liu *et al*., 2024; Nasato *et al*., 2021). Instead of representing rice grains as biaxial ellipsoid particles, the physical and chemical properties of rice grains are studied in the coarse-grained dynamics simulation using aggregates of rigid particles. Furthermore, we used compression simulations to examine the relationship between the grain-filling structure and mechanical properties of the rice ball. Thus, the molding conditions, grain-filling structure, and mechanical properties of rice balls with arbitrary food textures can be predicted by comparing the simulation results with the measured physical and chemical properties.

We aim to clarify the relationship between the rice grain-filling structure and mechanical properties of the rice ball by observing changes in the filling structure during compression using a model that reflects the measured physical and chemical properties of rice grains and ball in a coarse-grained dynamics simulation. We focus on the causal relationships between: (1) the molding conditions of the rice ball and grain-filling structure, (2) the grain-filling structure and food texture; and (3) the mechanical properties of the rice ball and food texture.

Materials and Methods

Sample Preparation Polished japonica rice (cultivar 'Hitomebore' harvested in Mizusawa, Iwate Prefecture, Japan, in 2020, Junjomai Iwate Co.) was cooked in deionized water. Edible grease (Molycote HP grease HP-500, Toray Dow Corning, Inc.) was used to reduce friction between rice grains and the inner wall of the mold. Propylene glycol (special grade reagent, FUJIFILM Wako Pure Chemicals Corp.) was used to measure the volume of rice grains, and 0.5 mol/L iodine solution (for volume analysis 094-01705, FUJIFILM Wako Pure Chemicals Corp.) was used as a contrast agent to measure the coordination number and contact area.

Polished rice (0.32 kg) was placed in a stainless-steel bowl (SUS304, φ 185 × H 70 mm), and 400 mL of deionized water at 25 °C was added. The mixture was stirred 10 times, and the starched water was replaced with fresh deionized water. This process was repeated five times. To prepare cooked rice samples with different water content, deionized water at 25 °C was added at three levels (1.2, 1.4, and 1.6 times the mass of polished rice), including water adsorbed by the washed rice. The rice was placed in a low temperature incubator (LTI-601SD, Tokyo Rika Kikai, Ltd.) set at 25 °C for 60 min. The soaked polished rice was then cooked in a rice cooker (Pressure IH Rice Cooker JPB-G180KL, Tiger Corp.) at "White Rice" setting. After cooking, the rice was steamed for 15 min and then stored in a temperature and humidity chamber (PL-1SP, Espec Corp.) set at 40 °C for 60 min for temperature adjustment.

To prepare the cylindrical rice ball, we used an acrylic resin-molded ring and a lid as shown in Fig. 1. Edible grease was applied inside the molded ring and the bottom of the push-on lid to prevent adhesion of rice grains. The ring was placed on an acrylic resin plate covered with food wrap film (Saran Wrap, Asahi Kasei Home Products Corp.). Rice balls were prepared at five rice grain fillings (20, 22, 24, 26, and 28 g) and five compression speed levels (0.1, 0.5, 1, 5, and 10 mm/s) using a uniaxial compression-tensile rheometer (RE-3305S, Yamaden Co., Ltd.), equipped with a 196-N load cell and a disk-type plunger (No. 19, φ 55 mm × H 8 mm) with an attached push-lid. Using rice grains with different water contents, three types of cylindrical rice balls (φ 40 mm × H 20 mm) with different void fractions were prepared: 20.0 g of rice grains compressed at 10 mm/s; 24.0 g of rice grains compressed at 1 mm/s; and 28.0 g of rice grains compressed at 0.1 mm/s. In a preliminary experiment, bulk density was measured immediately after compression molding and after 10, 30, and 60 minutes at 20 °C to see how the bulk density of the

J-Stage Released Online Advance Publication: February 21, 2025

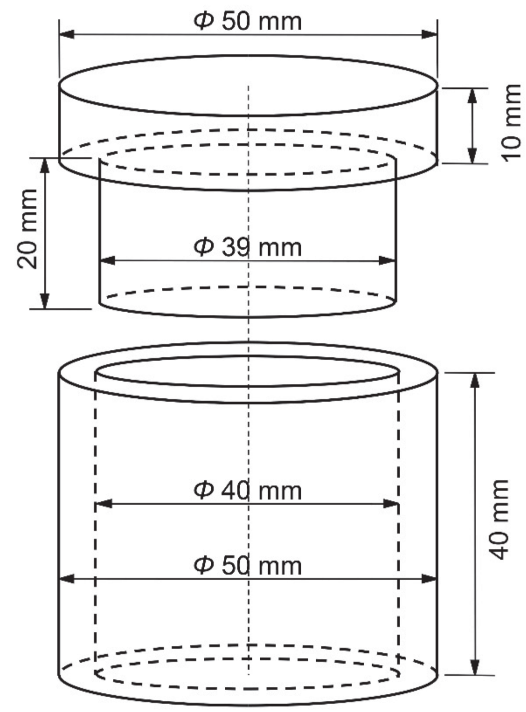

Fig. 1. Shaping mold for the preparation of rice ball.

rice mass changed over time. Based on the results of previous studies, the filling amounts were set to 24 g and 28 g of rice grains, which were considered to be appropriate for the size of the shaping mold. Stresses during compression molding ranged from 2 to 5 kPa, depending on the amount of rice to be filled into the shaping mold. Five minutes after the compression molding was completed, the rice mass was removed from the shaping mold. There was no significant change in the bulk density (0.82 ± 0.01–0.87 ± 0.02 g/cm^3) of any of the rice balls over time. Therefore, we considered that the rice balls underwent stress relaxation during the rice ball molding process.

Physicochemical Characterization of Rice Grains and Rice Balls The moisture content [% (w/w)] of the rice grains was measured using an infrared moisture tester (FD-800, Kett Electric Laboratory Co. Ltd.) with the measurement set to "auto stop" mode and the drying temperature set to 105 °C. The measurement was terminated when the change in moisture within 30 s reached 0.05 %.

For the rice grain imaging, five grains were pasted in a row on black drawing paper (W 50 mm × D 60 mm). Digital images (1024 × 768 pixels) were acquired at a magnification of 30 × using a high-speed microscope (consisting of a VW-9000 main unit, VH-20W zoom lens with 20 × to 200 × magnification, and a VH-S30B free angle observation system, Keyence Corp.). The longitudinal and transverse long and short axis lengths were measured from the two-dimensional images using image analysis and a measurement software

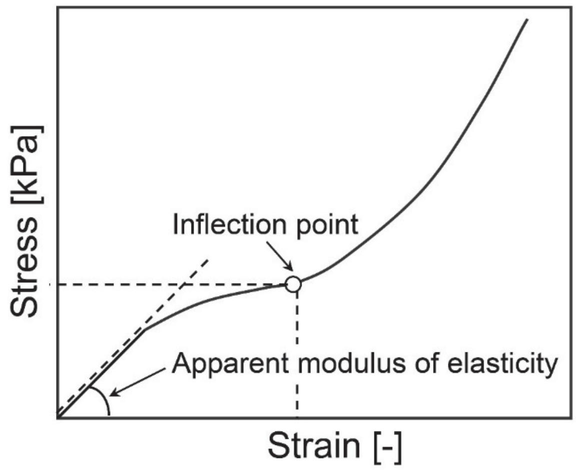

Fig. 2. Definition of apparent modulus of elasticity and inflection point in stress-strain curve.

(Image-Pro Primer Ver. 9.0, Hakuto Co., Ltd.).

Constant-speed compression tests were performed at a rate of 1 mm/s, maximum strain of 0.8, and data acquisition frequency of 100 Hz using a second uniaxial compression-tensile rheometer (RE2-33005C, Yamaden Co., Ltd.) equipped with a 19.6-N load cell and a cylindrical plunger (No. 5, φ 5 × H 22 mm). The apparent modulus of elasticity (in kPa) and inflection point of the rice grains were measured as defined in Fig. 2. The slope of the linear region of the stress-strain curve near the origin (elastic region) is defined as the elastic modulus. However, the rice grain is a biaxial ellipsoid, and the surface of the rice grain in contact with the plunger is curved when the major axis of the contour is set parallel to the sample table. Therefore, in the initial stage of compression, the plunger and rice grains shift from point contact to surface contact. Therefore, the modulus of elasticity was calculated using the contact area between the plunger and the rice grains as the cross-sectional area of the plunger, which was defined as the apparent modulus of elasticity. The inflection point was defined as the point at which the stress-strain curve changes from convex upward to convex downward. To prevent hardening of the rice grain surface due to drying, the rice grains were placed in a glass desiccator (φ 120 mm × H 200 mm, bottom filled with 100 mL deionized water) set in a constant-temperature water bath (NTT-2100, Tokyo Rika Kikai, Co., Ltd.) at 40 °C. Measurements were done quickly after the rice grains were removed from the desiccator.

Four rice grains were arranged in two rows by two columns on a paper wiper (Kimwipe S-200, 20 mm × 20 mm, Nippon Paper Crecia Co., Ltd.), and one rice grain was placed on top of the four grains. Constant-velocity extension tests were conducted using another uniaxial compression-tensile rheometer equipped with a 1.96-N load cell and a disk-type

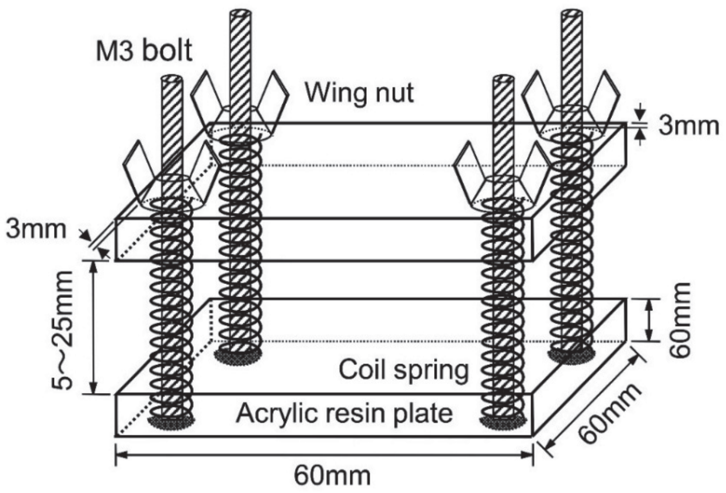

Fig. 3. Compressing device for the rice ball.

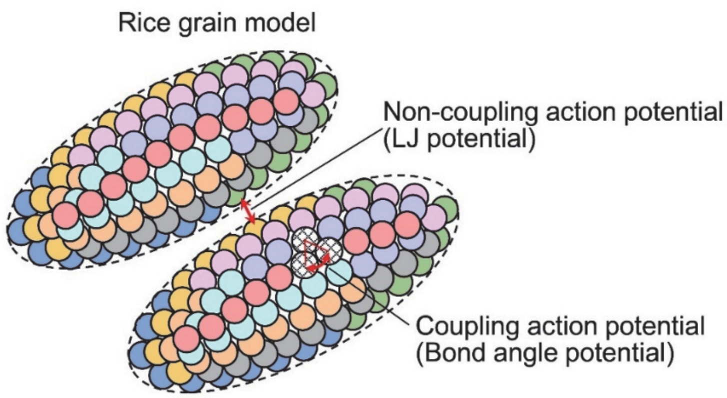

Fig. 4. Rice grain model for the coarse-grained dynamics simulation.

plunger (No. 2, φ 40 mm × H 8 mm) at an extension rate of 1 mm/s, strain of 0.8, data acquisition frequency of 100 Hz, and precompression loads of 40, 80, and 120 mN. The maximum tensile force obtained was used as the adhesion force. Since the measured mechanical properties of the rice grains vary greatly depending on the dryness of the grains, we only used data obtained within 90 s after the rice grains were first laid out.

The subsequent cylindrical rice balls were weighed, and their volumes were measured using a laser volumetric measuring system (SELNAC-WinVM2100, K-AXIS Co., Ltd.). Meanwhile, the rice grain volume was measured by the immersion method using 50 mL of propylene glycol. From the measured volumes of the rice ball and grains, the void fraction of the rice ball was calculated using Equation (1).

Void fraction [%] = 1 – (Volume of rice grain) / (Volume of rice ball) × 100 (1) ······ Eq. 1

Rice ball samples with significantly different void fractions were prepared by compressing them using the rice ball compressing apparatus shown in Fig. 3. A desktop microfocus X-ray CT system (inspXio SMX-90CT, Shimadzu Corp.) was used to obtain 3D images of the rice ball and measure the coordination number and contact area. The images were taken with a slice thickness of 2 mm, 3000 slice views, and a scaling factor of 50, and four images were averaged to get the final image. The coordination number and contact area were measured using an image analysis software (VGStudio MAX, Volume Graphics GmbH).

To get the stress-strain curves, a constant-speed compression of the rice ball was performed using a uniaxial compression-tensile rheometer equipped with a 1.96-N load cell and a disk-type plunger (No. 19, φ 55 mm × H 8 mm) at a compression rate of 1 mm/s, a maximum strain of 0.8, and a data acquisition frequency of 100 Hz. The stress and strain were measured at the inflection point (at the transition from elastic to plastic deformation).

Coarse-grained Dynamics Simulations A rice grain model (Fig. 4) was created by a coarse-grained dynamics simulation method using the material property simulation software J-OCTA (version 9.1, JSOL Corp.). A rice grain model consisting of 125 rigid particles was created by first cutting a cubic model into a shape similar to an actual rice

J-Stage Released Online Advance Publication: February 21, 2025

grain before cutting out the grain model consisting of 4 000 rigid particles (10 cells containing four rigid particles in each of the three directions). The rice grains are modeled as an aggregate of rigid particles, and the bond angle parameters between rigid particles and the Lennard-Jones (LJ) potential between non-bonded particles are adjusted to represent the physicochemical properties of the rice grains. The cutoff parameter of the LJ potential was used to set the attraction or repulsion. By changing their strength and range of action, the adhesion force between grain models due to compression can be set.

One rice grain model was isotropically compressed and randomly oriented to create a rice grain-filled model with three-unit voxels in each of the three axes ($3^3 = 27$). For a realistic model, the rice grain was oriented randomly rather than compress the biaxial ellipsoid grain model while oriented in a one direction. Moreover, instead of duplicating each rice grain model, the unit voxels of the rice particle filling model containing one rice grain model are duplicated and arranged in a 3 × 3 grid. Therefore, since the rice grain models reside in the unit voxel of the grain-filling model and the solver is used to randomize the orientation within the unit voxel, there is no bias in the spatial arrangement of the 27 rice grain models; only the orientation is random. For triaxial compression, one vertex in the cubic cell of the grain-filling model was set to be spatially fixed for equidirectional compression, with temperature 298 K, cell compression pressure 0.8 kPa, LJ potential cutoff 2.5 (gravitational setting), and $\varepsilon = 1.0$ eV(force magnitude parameter due to LJ potential).

The rice grain-filling model was used to perform uniaxial constant-velocity compression simulations. In the compression simulation, the bond angle potential K corresponds to the rice grain hardness, the ε value of the LJ potential corresponds to the adhesion force of the rice grain, the free volume fraction as the space fraction of the rice ball model, and the elongation rate of the rice ball model as the compression rate. The stresses on the compression surface were calculated for each parameter. In all models, the cells were deformed after relaxation calculations to reflect the set values.

Compression simulations were performed for a set of models with varying bond angle potential K (Simulation 1). The potential K is given to the angle between the two bonds connecting the three rigid particles that make up the rice grain model and can be set to determine the resistance to changes due to compression. By setting the K value, the deformability and hardness of the rice grain model was defined. The simulations were performed with a time step of 0.001 for 400 000 time steps with values were output every 1 000 steps. The solver was set to a parameter representing the condition of constant volume and temperature and with thermal energy output and input (NVT_Kremer_Grest). Moreover, the compressive force was set to Max_Force = 1.0×10^9, deformation mode was set to Simple_Elongation in Cell_Deformation. The compression was set to be only along z with Compression_Rate = 0.005, Poisson_Ratio = 0.2, and free volume fraction before compression set to 30 %. Nine levels of K were considered (10, 50, 100, 125, 150, 175, 200, 500, and 1 000) along with an LJ potential cutoff of 2.5 (gravitational setting) and ε=1.0. Stresses during compression were subsequently examined for the rice grain models of varying hardness.

Compression simulations were also performed for rice grain models with different adhesion forces (i.e., varying ε values, Simulation 2). The ε value is the potential acting on unbonded rigid particles, and the cutoff parameter can be set for either attraction or repulsion. By changing their strength and range of action, the adhesion force between rice grain models due to compression can be set. Time settings, solver, compressive force, deformation mode, deformation rate, deformation direction, Poisson's ratio, and free volume fraction before compression were set to the same values listed in Simulation 1. Four ε values were considered (0.5, 1.0, 1.5, and 2.0) while the bond angle potential was fixed at K = 100 and Cutoff = 2.5 (the attraction setting). The subsequent compressive stresses were examined for the rice grain models with different adhesion forces.

For Simulation 3, compression simulations were performed for models with varying free volume fraction (i.e., different void fractions). The free volume fraction is the ratio of the space in which rigid particles of a specified size can move freely in a cell containing 27 rice grain models. Since the space within the rice grain model consisting of 125 rigid particles was not considered, it is suitable for expressing the void fraction of a rice ball. Time settings, solver, compressive force, deformation mode, deformation rate, deformation direction, and Poisson's ratio were set to the same values listed in Simulation 1. Six levels of free volume fraction before compression were set: 20; 25; 30; 35; 40; and 45 %. Moreover, Cutoff = 2.5 (gravitational setting), ε = 1.0, and K = 100 for the LJ potential. This simulation was used to study the effect of void fraction on stress during compression.

Lastly, compression simulations were performed for a group of models with different compression rates (determined by the Simulation 4 parameter Elongation_rate). Elongation_rate sets the size of cells to be deformed in one step and can be set to positive and negative values for tension and compression, respectively. In the deformation mode called Simple_Elongation, the cell can be deformed in uniaxial and biaxial directions, thus simulating a compression rupture test of a real rice ball. The total time steps and output interval steps were set to six levels: Total_Steps = 4 000 000, 2 000 000,

Table 1. Geometry of cooked rice grain.

Mass ratio of water to rice grain	Major axis of longitudinal section [mm]	Major axis of transverse section [mm]	Minor axis of transverse section [mm]
1.2	7.41 ± 0.85	3.20 ± 0.19	1.95 ± 0.19
1.4	7.44 ± 0.39	3.15 ± 0.12	2.23 ± 0.13
1.6	8.76 ± 0.19	3.23 ± 0.12	2.27 ± 0.14

Mean ± standard deviation (n = 5)

Table 2. Adhesion force [kN] of cooked rice grain.

Mass ratio of water to rice grain	Preload force [mN]		
	40	80	120
1.2	0.08 ± 0.01[abc]	0.12 ± 0.01[d]	0.12 ± 0.02[d]
1.4	0.07 ± 0.01[ab]	0.10 ± 0.01[cd]	0.12 ± 0.02[d]
1.6	0.06 ± 0.01[a]	0.10 ± 0.01[cd]	0.11 ± 0.02[d]

Mean ± standard deviation (n = 5)
Values followed by the same letter are not significantly different (p < 0.05).

400 000, 200 000, 40 000, and 20 000; Output_Interval_Steps = 10 000, 5 000, 1 000, 500, 100, and 50; and delta_T = 0.001, so that all output records fit into 400 records. The solver, compressive force, deformation mode, deformation direction, Poisson's ratio, and free volume fraction before compression were set to the same values listed in Simulation 1. The Compression_Rate was set to six levels: 0.0005; 0.001; 0.005; 0.01; 0.05; and 0.1. The rest of the parameters of the rice grain model were set to the values described in Simulation 3. This simulation was used to study the effect of compression rate on stress.

Statistical processing and analysis Statistical analysis software (IBM SPSS Statistics Desktop for Japan Ver. 27.0, IBM Japan, Ltd.) was used for the calculation of basic statistics and statistical testing.

Results and Discussion

Physicochemical Properties of Rice Grains and Rice Balls The moisture content of the polished rice before cooking was 12.88 % (w/w), and that of the cooked rice with 1.2, 1.4, and 1.6 times the amount of water added was 52.33, 57.89, and 61.02 % (w/w), respectively. The grain size tended to increase with the water content (Table 1) due to the increased water absorption and swelling during cooking. Furthermore, the apparent modulus of elasticity of cooked rice with 1.2, 1.4, and 1.6 times the amount of water added was 100.4 ± 4.2, 70.0 ± 9.2, and 60.8 ± 6.6 kPa, respectively. The decrease in the modulus of elasticity with increasing moisture content in the rice grains was attributed to an increase in the water content acting as a plasticizer, as well as to an increase in the degree of swelling, a decrease in density, and an increase in specific volume. Moreover, the adhesion force of rice grains increased with the precompression load, but seemed to be independent of the amount of added water (Table 2). The texture of Koshihikari (*Oryza sativa* L.) not easily changed by the water-to-rice (W/R) ratio, and the optimum W/R ratio was found to be × 1.4 because of low firmness and high adhesiveness (Tamura *et al.*, 2024). The decrease in firmness and increase in adhesiveness as the W/R ratio increases can be attributed to an increase in the degree of gelatinization with a prolonged cooking time, damage to cellular tissue due to differences in swelling pressure caused by differences in water absorption inside and outside of the grain, and coating of solids eluted from the grains on the surface of the cooked grains. Therefore, it is considered that the W/R ratio in this study was set without any change in adhesion. Moreover, the decrease in the rice grain density did not affect the adhesiveness of the rice grains.

Table 3 shows the void fraction of rice ball with 1.4 times water content as a function of the forming conditions. Faster molding speed increased the space ratio due to the elastic behavior of the rice grains, which return to their original shape rather than fill the space as the compression speed increases. On the contrary, the rice grains behave more viscously for slower compression speeds, and the grains tend to fill the gaps between rice grains; thus, the grain volume decreases and does not elastically recover. Furthermore, increasing the amount of water added during cooking tended to decrease the void fraction as shown in Table 4 for different masses of rice, compression speeds, and water-to-rice mass ratios. Therefore, increasing the water content increased the rice grain volume during cooking, lowering the space factor. These differences in void fractions would change the surface characteristics of the rice grain (*e.g.*, unevenness, adhesiveness, and coefficient of friction), which may lead to changes in food texture and palatability, such as stickiness and hardness.

Meanwhile, Table 5 shows no significant relationship between the coordination and compression speeds for rice

J-Stage Released Online Advance Publication: February 21, 2025

Table 3. Difference in void fraction of rice ball cooked with mass ratio of water to rice grain of 1.4 depending on molding conditions

Filled cooked rice	Compression speed [mm/s]				
[g]	0.1	0.5	1	5	10
20	0.250 ± 0.016^{ab}	0.392 ± 0.010^{ef}	0.382 ± 0.033^{ef}	0.407 ± 0.019^{f}	0.379 ± 0.021^{ef}
22	0.204 ± 0.029^{ah}	0.360 ± 0.015^{de}	0.382 ± 0.017^{ef}	0.378 ± 0.010^{ef}	0.366 ± 0.017^{def}
24	0.194 ± 0.031^{h}	0.326 ± 0.014^{cd}	0.330 ± 0.021^{cd}	0.354 ± 0.024^{de}	0.356 ± 0.007^{de}
26	0.178 ± 0.013^{gh}	0.289 ± 0.014^{bc}	0.329 ± 0.009^{cd}	0.251 ± 0.018^{ab}	0.303 ± 0.014^{c}
28	0.162 ± 0.011^{gh}	0.145 ± 0.009^{g}	0.286 ± 0.002^{bc}	0.298 ± 0.008^{g}	0.284 ± 0.014^{bc}

Mean ± standard deviation ($n = 5$)
Values followed by the same letter are not significantly different ($p < 0.05$).

Table 4. Difference in void fraction of rice ball depending on cooking condition.

Filled cooked rice	Compression speed	Mass ratio of water to rice grain		
[g]	[mm/s]	1.2	1.4	1.6
20	10	0.423 ± 0.009^{a}	0.379 ± 0.021^{e}	0.317 ± 0.013^{e}
24	1	0.345 ± 0.012^{de}	0.330 ± 0.021^{d}	0.272 ± 0.011^{c}
28	0.1	0.263 ± 0.016^{c}	0.162 ± 0.011^{b}	0.186 ± 0.012^{b}

Mean ± standard deviation ($n = 5$)
Values followed by the same letter are not significantly different ($p < 0.05$).

Table 5. Difference in coordination number of rice grain depending on molding conditions.

Filled cooked rice	Compression speed [mm/s]				
[g]	0.1	0.5	1	5	10
20	6^{abcde}	6^{abcde}	6 ± 1^{bcde}	8 ± 1^{bcde}	8 ± 1^{e}
22	7 ± 1^{de}	6 ± 1^{ab}	7 ± 1^{abcd}	5^{abc}	7 ± 1^{a}
24	8^{de}	6 ± 1^{abcde}	7 ± 1^{a}	6^{abcde}	5 ± 1^{abcde}
26	7 ± 1^{abcde}	6 ± 1^{abcde}	7 ± 1^{abcde}	5^{abcde}	7^{abcde}
28	7 ± 1^{abcde}	6^{abcde}	8 ± 1^{de}	5 ± 1^{cde}	7 ± 1^{bcde}

Mean ± standard deviation ($n = 5$)
Values followed by the same letter are not significantly different ($p < 0.05$).

Table 6. Difference in coordination number of rice grain depending on molding conditions.

Filled cooked rice	Compression speed	Mass ratio of water to rice grain		
[g]	[mm/s]	1.2	1.4	1.6
20	10	5 ± 1^{a}	6^{ab}	5 ± 1^{a}
24	1	5 ± 1^{a}	7 ± 1^{b}	6 ± 1^{ab}
28	0.1	6 ± 1^{ab}	7 ± 1^{ab}	6 ± 1^{ab}

Mean ± standard deviation ($n = 5$)
Values followed by the same letter are not significantly different ($p < 0.05$).

cooked with 1.4 times the water content. Moreover, the coordination number did not significantly change even with varying amounts of water added, as shown in Table 6. Nevertheless, the contact area between adjacent rice grains increased as the amount of filling and amount of water increased (Fig. 5). The rice grains with 1.6 times added water had a softer surface layer and flowed plastically, which caused the rice grains to extend in the direction of movement, increasing the contact area. In the case of 1.2 times added water, the rice grains were in point contact with neighboring rice grains.

Figure 6 shows the effect of molding conditions on the mechanical properties of the rice balls made from rice cooked with 1.4 times added water. For the same compression rate, the stress at the inflection point increased as the amount of rice filling into the mold increased. For the same amount of filling, the stress at the inflection point increased for slower molding speeds. This is similar to the change in the void fraction (Table 3), where the stress at the inflection point was inversely proportional to the void fraction. In this work, the inflection point stress refers to the stress required for the internal collapse of the rice mass. Rice balls with a high void fraction

J-Stage Released Online Advance Publication: February 21, 2025

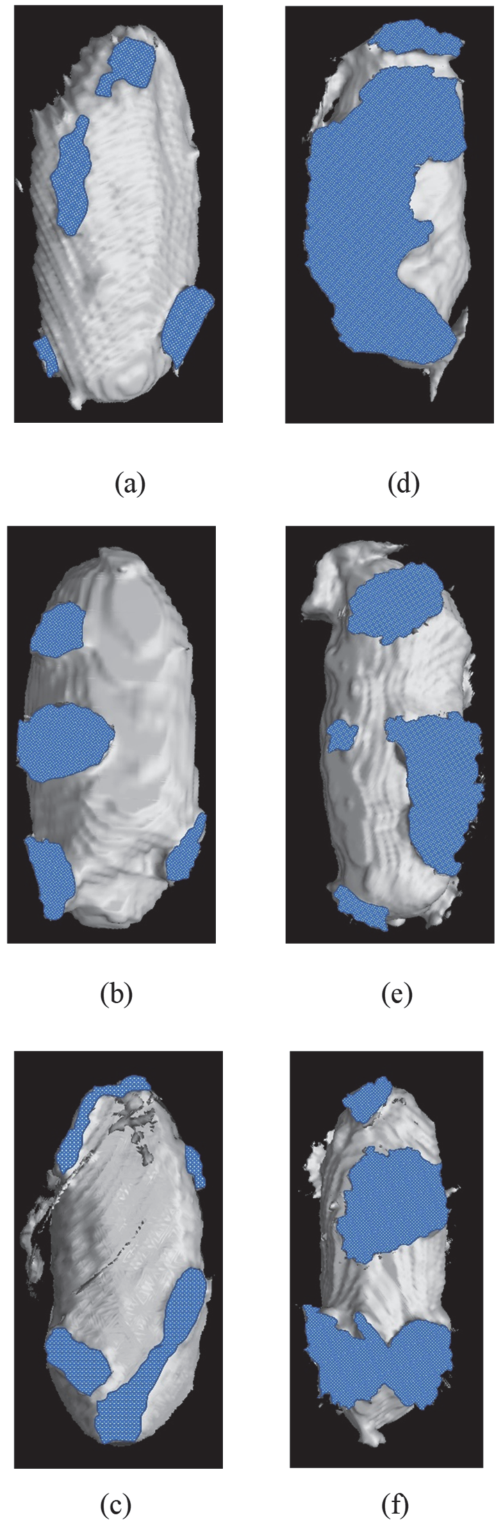

Fig. 5. Rice grain contact area observed by X-ray CT as a function of water-to-rice mass ratio, cooked rice mass, and compression speed, respectively: a) 1.4, 20 g, 10 mm/s; b) 1.4, 24 g, 1 mm/s; c) 1.4, 28 g, 0.1 mm/s; d) 1.6, 20 g, 10 mm/s; e) 1.6, 24 g, 1 mm/s; and f) 1.6, 28 g, 0.1 mm/s. Blue shaded areas indicate contact areas.

are brittle and easily collapses because there is a lot of space between rice grains constituting the rice ball, while rice balls with a low space factor are difficult to collapse because the rice grains are densely constituted, increasing the stress required for collapse. The inflection point strains were from 0.2 to 0.3, which were the same for all rice balls, indicating that internal collapse occurred at the same strain.

Figure 7 shows the effect of the preparation conditions on the mechanical properties of the rice balls with 1.2, 1.4, and 1.6 times added water. The stress at the same strain and at the inflection point were higher in the cooked rice ball with 1.2 times added water than those for 1.4 and 1.6. This is because the apparent modulus of elasticity was higher for rice grains cooked with less added water; therefore, compressing them requires greater force. For rice balls with 1.6 times added water, the rice grain surface is soft and easily deformable, so the rice grains do not fill the void but rather deform plastically in the direction of compression. The three-dimensional arrangement of the rice grains in the rice ball is maintained when compressed, and the stress is slightly higher than in the case of 1.4 times added water.

Uniaxial Compression Simulations: *Varying Hardness* The rice grain models did not attract each other strongly and moved while sliding when the LJ potential ε for all grain models was fixed at 1.0 and the attraction between rice grain models was set to low (Fig. 8). For the rice grain models with K = 10 and 50, deformation started when the rice grain model moved to some extent, and the model was compressed up to the maximum compression force Max_Force. For rice grain models sliding against each other, the stress did not decrease rapidly because of the very low hardness of the rice grain models; thus, the outer surfaces of the grain models were slightly deformed when they overlapped each other. Finally, the rice grain models were deformed to fill the space without maintaining their original forms. In the rice grain models with $K = 100$ and 200, the model started to deform after sliding and reached Max_Force with several displacements. This behavior was also observed in actual rice grains, and the shapes of the stress-strain curves from measurements and simulations were similar. In both models, the rice grain model began to deform around 0.6 in strain, with no space for the rice grain model to move, and the stresses increased rapidly. The stress in the rice grain model with $K = 200$ was greater than that in the rice grain model with $K = 100$. The compressive deformation of the rice grain model above a strain of 0.6 was a result of the rice grain model being crushed when $K = 100$, but the deformation was suppressed when $K = 200$, and the rice grain model moved more frequently, increasing the strain and stress until Max_Force was reached.

The rice grain model with $K = 500$ and 1 000 remained a biaxial ellipsoid and was compressed while being displaced

J-Stage Released Online Advance Publication: February 21, 2025

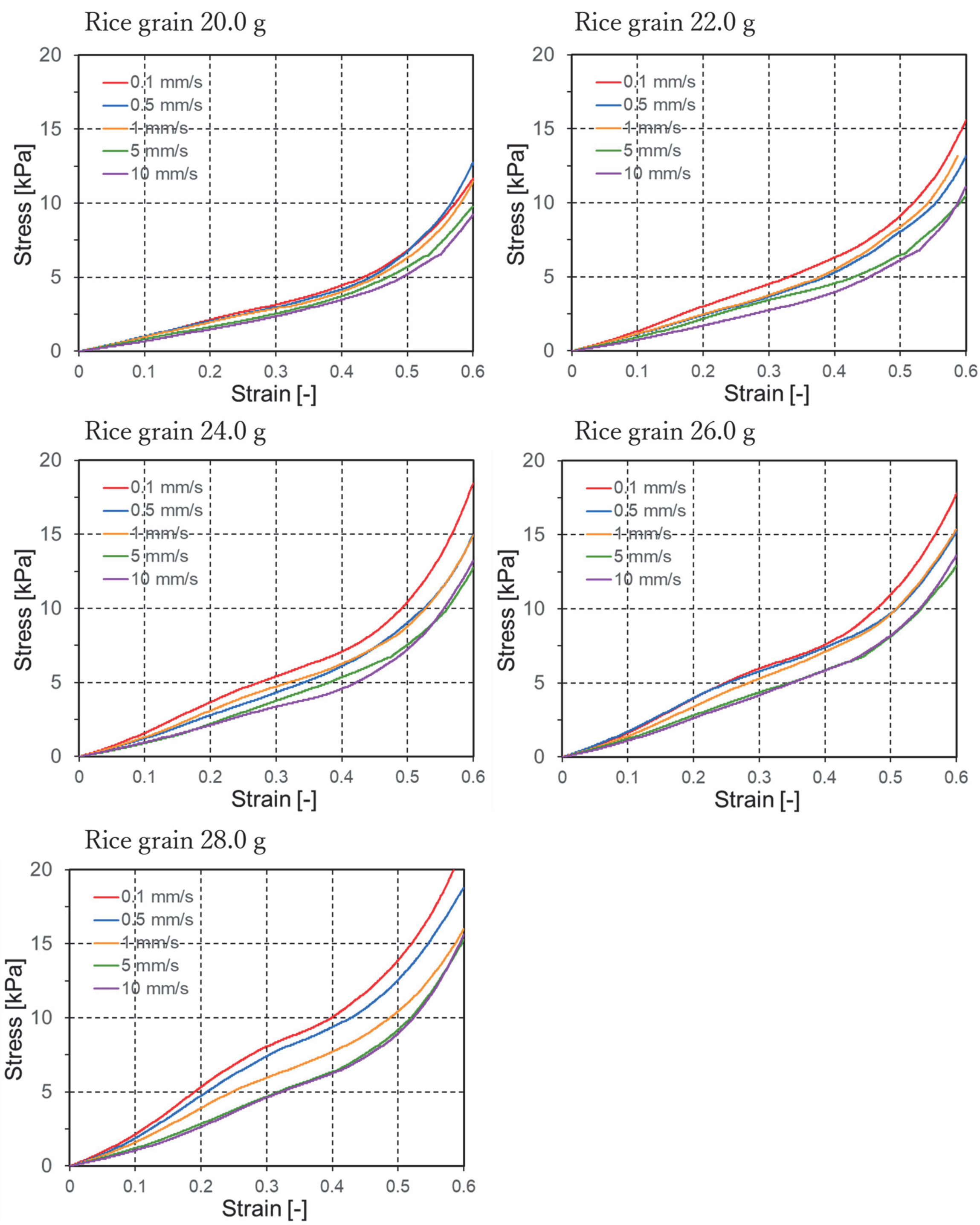

Fig. 6. Effect of varying rice filling mass and compression speeds on the stress-strain curves of rice ball cooked with a 1.4 water-to-rice mass ratio. Compression speeds of 0.1 mm/s, 0.5 mm/s, 1 mm/s, 5 mm/s, and 10 mm/s were used for rice balls prepared with 20.0 g, 22.0 g, 24.0 g, 26.0 g, and 28.0 g of rice grains, respectively.

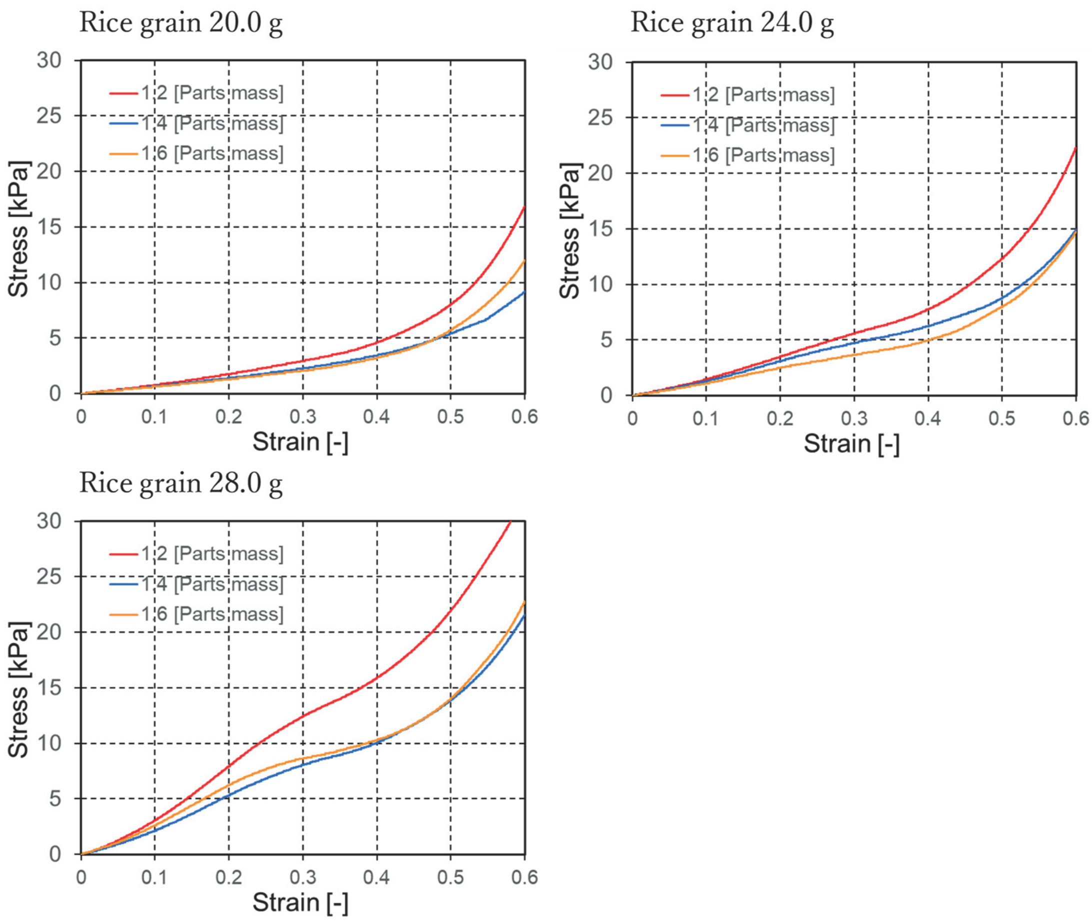

Fig. 7. Stress-strain curves of rice balls with varying water-to-rice mass ratio and rice filling mass. Compression speeds of 10 mm/s, 1 mm/s, and 0.1 mm/s were used for rice balls prepared with 20.0 g, 24.0 g, and 28.0 g of rice grains, respectively.

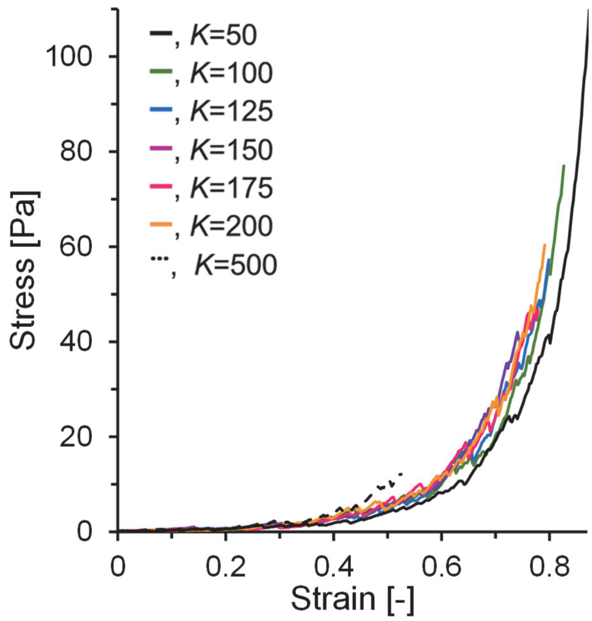

Fig. 8. Effect of K on the stress-strain curves of rice ball models at a compression rate of 0.005, void fraction of 0.3, and ε of 1.0.

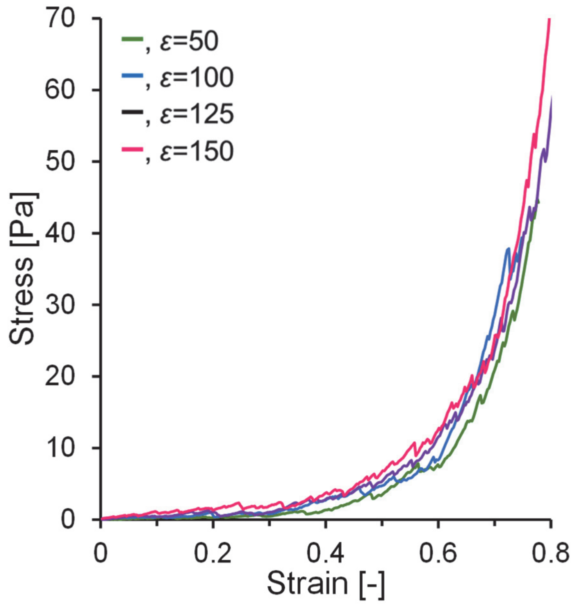

Fig. 9. Effect of ε on the stress-strain curves of rice ball models at a compression rate of 0.005, void fraction of 0.3, and *K* of 100.

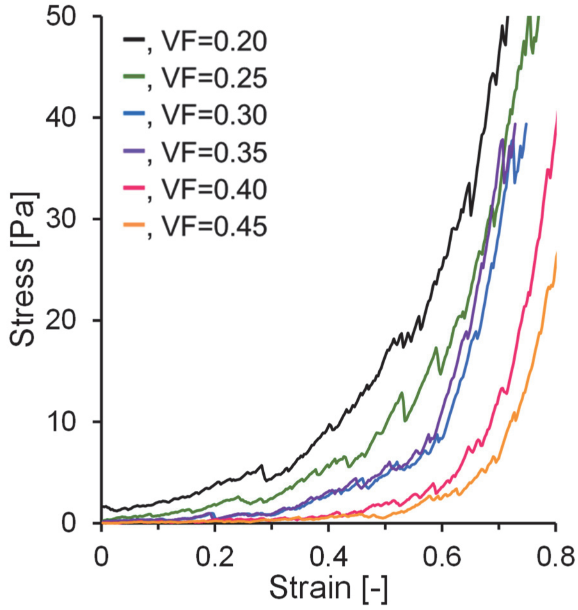

Fig. 10. Effect of *K* on the stress-strain curves of rice ball models at a compression rate of 0.005, void fraction of 0.3, and ε of 1.0.

many times. Since the rice grain model was compressed without moving due to the loss of space for movement at around 0.5 strain, Max_Force was quickly reached, resulting in a completely different behavior from that of the actual measurement. These results suggest that the *K* value that reflects the behavior of actual rice grains is around 100 to 200. Therefore, rice grains can be simulated with different hardness by changing *K* to 100, 125, 150, 175, and 200. In all rice grain-filled models, the grain model frequently moved in a sliding manner during compression. Upon losing space to move, the rice grain model was compressed while deforming. The rice grain model with *K* = 100 and 125 was easily deformed and compressed such that the deformation and movement were repeated many times.

Uniaxial Compression Simulations Varying Particle Adhesion Forces When the LJ potential ε was increased, the attraction between grain models in contact became stronger, which suppressed the movement of the grain models during compression and maintained the particle-filled structure. The stress on the compression surface increased in the initial stage of compression, as shown in Fig. 9. This increase in stress is due to the retention of the three-dimensional arrangement of the rice grains, similar to the compression test of rice balls using rice with 1.6 times added water. Changing the values of the bond angle and LJ potentials allows for rice grain compression simulations that reflect the different physicochemical properties of rice grains as a function of rice variety and cooking conditions (e.g., amount of water added, soaking time, temperature and pressure profiles).

Uniaxial Compression Simulations: Varying Space Factors By increasing the free volume fraction, the rice grain models moved into the gaps between rice grain models during compression, and the stress against the compression surface did not increase easily (Fig. 10). In the grain-filling model with a small free volume fraction, the stress increases from the low strain region, whereas in the grain-filling model with large free volume fraction, the deformation progresses and the stress increases from a strain of 0.4, indicating that the rice grains move to fill the space in the initial stage of compression. This was considered to be similar to the change in stress with the space factor of the rice mass.

Uniaxial Compression Simulation: Varying Compression Speeds In the grain-filling model with a high compression speed, the grain model could not move sufficiently during compression because the compression speed was faster than the speed at which the rice grain model moved during compression (Fig. 11). Compression progressed with almost no decrease in stress as the rice grain model moved, which is an expected behavior for actual rice balls. On the contrary, in the model with a slower compression speed, the grain model moved faster than the compression speed during compression, frequently moving the rice grain models into the gap, which decreased the stress. These results are similar in actual measurements. Therefore, the rice grain movements are controlled by the physicochemical properties of the rice grains. When the movement speed exceeds the compression speed, the

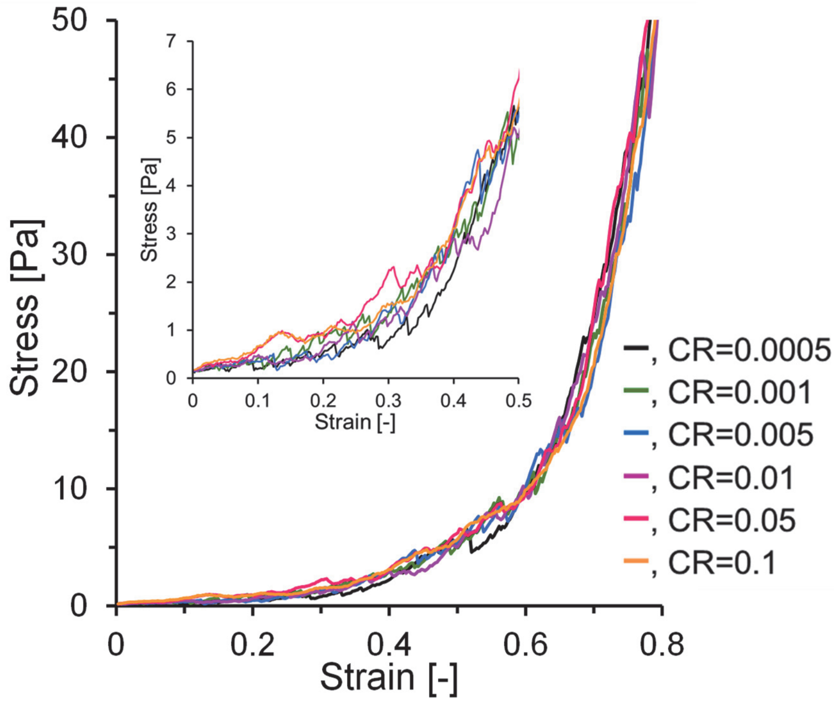

Fig. 11. Effect of compression rate (CR) on the stress-strain curves of rice ball models at a void fraction of 0.3, ε of 1.0, and K of 100. The inset figure shows an enlarged view of the region from strain values of 0 to 0.5.

rice grains move into the gaps between rice grains. Meanwhile, when the compaction rate exceeds the movement rate, or when the space available for movement is lost, the rice grains themselves are deformed and compaction proceeds. In addition, when the rice grain model was deformed, a gap was created where the rice grain model could move further, decreasing the stress. This behavior was also assumed to occur in actual measurements. The grain-filling model in this study assumes 27 grains in the center region of the actual rice ball and applies a periodic boundary surface, which is a surface that is spatially connected to a face and its counterpart. The rice grain models placed in the wall section of the cell were separated by periodic boundary surfaces, but were able to move to the space opposite to them, so there were many spaces where they could move laterally. On the contrary, the rice grain model in the center region of the cell moved to the upper and lower spaces, or to the space created by the rice grain model on the cell wall moving out of the cell, because there was little space to move left and right. The movement of the rice grain model at the wall and center region of these cells was consistent with the movement of rice grains during compression process obtained from X-ray CT imaging of actual rice balls. The presence of rice grains in the cross section at half the height of the cylindrical rice ball was compared (Fig. 12). Rice grains in the central region in the top view image appeared to move horizontally as if filling the void. On the other hand, in the outer end region, the rice grains appeared to move towards the outer end as the compression progressed.

As mentioned above, the coarse-grained dynamics simulation using the grain-filling model in this study was able to simulate the behavior of rice grains during actual rice ball compression.

Therefore, given the successful coarse-grained dynamics simulations for the relationships between the rice ball-forming conditions, grain-filling structure, mechanical properties, and food texture, it is possible to develop a rice processing machine that can produce rice balls with ideal food texture for the consumer. Preliminary experiments (data not shown) have shown that the compression speed by the sushi chef is 350–700 mm/s in the first molding and 600–750 mm/s in the second molding. On the other hand, the upper limit of the compression speed in the coarse-grained kinetic simulation was also limited to 10 mm/s because the upper limit of the compression speed that could be set with the uniaxial compression/tension rheometer used in this study was 10 mm/s. The rice ball that showed the most similar disintegration behavior to that of the rice ball made by sushi chefs was a rice ball formed by filling a shaping mold with 22 g of rice grains and compressing it at a rate of 10 mm/s. This simulation provides a new approach to the relevant studies on the mechanical properties of rice balls by considering their behavior as grain-filling structure.

J-Stage Released Online Advance Publication: February 21, 2025

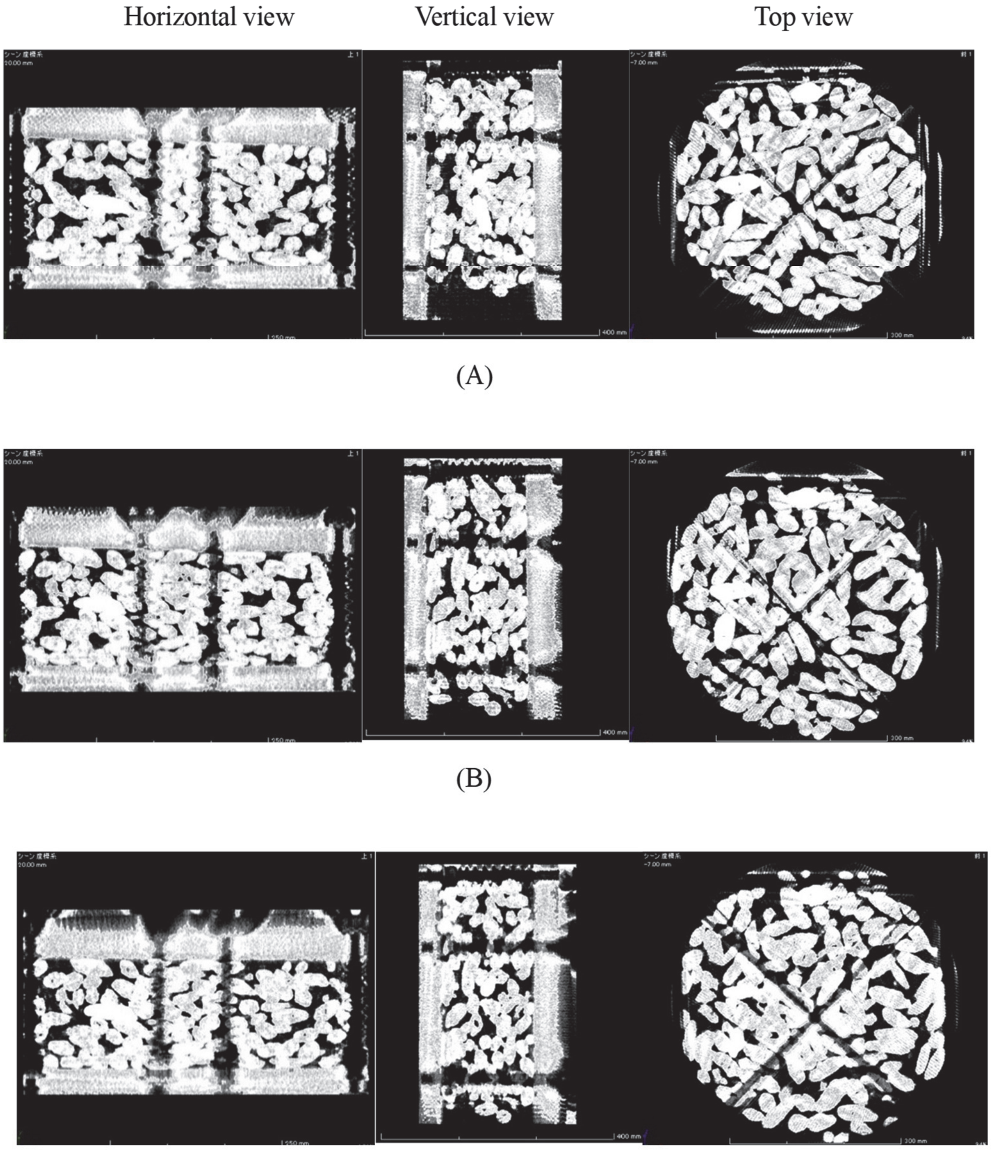

Fig. 12. Cross sectional images of rice ball obtained from X-ray CT system.
Sample were compressed at 0.20 (A), 0.25 (B) and 0.30 (C) of strain, respectively. Dark lines in the image indicate X-rays cannot be transmitted due to the presence of metal bolts in a compressing device for the rice ball as shown in Fig. 3.

Conclusion

Preparing rice balls with good food texture require measurement of the mechanical properties of the rice balls, taking into account the interaction forces acting on the individual rice grains and the grain-packing structure. However, the rice grain-filling structure cannot be arbitrarily changed, and the effects of filling structure on mechanical properties and food texture are unknown. Instead of representing each rice grain as a biaxial ellipsoidal particle, we used an aggregate of many rigid particles to model the physical and chemical properties of the rice grain in our coarse-grained dynamics simulation. The simulations were able to describe the behavior of rice grains during rice ball compression. The relationship between the grain-filling structure and mechanical properties of the rice balls, revealed by compression simulations, was clarified. Comparing the simulation results with the measured physicochemical properties allows us to predict rice ball-preparation conditions, grain-filling structure, and mechanical properties to express arbitrary rice ball textures.

Acknowledgements We would like to express our deepest gratitude to Kosuke Ohata of Engineering Technology Business Unit, JSOL Corp. for his great guidance in coarse-grained dynamics simulations and Moe Tanuma of Iwate University Research Support and Industry-Academic Collaboration Center for her help in measuring the coordination number and contact area of rice grains in a rice ball. We would like to thank Editage (www.editage.jp) for English language editing.

Conflict of interest There are no conflicts of interest to declare.

References

Chen, H., Rao, X., Zhang, G., Yang, G., Yang, G., Wang, X., and Hu, Y. (2024). Changes of eating quality of four types of rice with different amylose content under different storage temperatures. *Int. J. Food Sci. Technol.*, **59**, 5462–5468. doi:10.1111/ijfs.17262

Chen, Y., Zhu, M., Wang, X., Yan, Y., Ji, Q., Li, J., and Xia, S. (2024). Effect of electric cooker soaking temperature on palatability of cooked aged indica rice. *J. Cereal Sci.*, **118**, 103982. doi:10.1016/j.jcs.2024.103982

Chibrikov, V., Pieczywek, P.M., Cybulska, J., and Zdunek, A. (2024). Coarse-grained molecular dynamics model to evaluate the mechanical properties of bacterial cellulose–hemicellulose composites. *Carbohydr. Polym.*, **330**, 121827. doi:10.1016/j.carbpol.2024.121827

Derossi, A., Palma, E.D., Moses, J.A., Santhoshkumar, P., Caporizzi, R., Severini, C. (2023). Avenues for non-conventional robotics technology applications in the food industry. *Food Res. Int.*, **173**, 113265. doi:10.1016/j.foodres.2023.113265

Garofalo, M.A., Salazar, R., Palacios-Ponce, A., Cornejo, F., and Corradini, M.G. (2024). Rice storage under controlled conditions: Changes in its physicochemical and functional properties. *J. Stored Prod. Res.*, **105**, 102236. doi:10.1016/j.jspr.2023.102236

Kim, H. and Choi, J. (2024). Influence of crystalline structure on creep resistance capability in semi-crystalline Polymers: A coarse-grained molecular dynamics study. *Int. J. Fatigue*, **188**, 108517. doi:10.1016/j.ijfatigue.2024.108517

Kim, H., Kim, O-W., Kwak, H.S., Kim, S.S., and Lee, H-J. (2017). Prediction model of rice eating quality using physicochemical properties and sensory quality evaluation. *J. Sens. Stud.*, **32**, e12273. doi:10.1111/joss.12273

Kwak, H.S., Kim, M., Lee, Y., and Jeong, Y. (2015) Identification of key sensory attributes for consumer acceptance and instrumental quality of aseptic-packaged cooked rice. *Int. J. Food Sci. Technol.*, **50**, 691–699. doi:10.1111/ijfs.12684

Li, C., Ji, Y., Li, E., and Gilbert, R.G. (2023). Interactions between leached amylose and protein affect the stickiness of cooked white rice. *Food Hydrocolloids*, **135**, 100215. doi:10.1016/j.foodhyd.2022.108215

Li, L., Shi, S., Cheng, B., Zhao, D., Pan, K., Cao, C., and Jiang, Y. (2023). Association between rice protein components and eating quality traits of different rice varieties under different nitrogen levels. *J. Cereal Sci.*, **113**, 103760. doi:10.1016/j.jcs.2023.103760

Liu, J.H., Yu, Z., and Li, D.M. (2024). Role of terminal beads in fracture of topological gels: A coarse-grained molecular dynamics study. *Mater. Today Commun.*, **41**, 110341. doi:10.1016/j.mtcomm.2024.110341

Liu, X., Guo, Y., Wang, S., Wang, X., Wang, Z., and Wang, Z. (2024). Effects of ultrasound combined with hydrothermal treatment on the quality of brown rice. *LWT-Food Sci. Technol.*, **196**, 115874. doi:10.1016/j.lwt.2024.115874

Ma, M., Gu, Z., Cheng, L., Li, Z., Li, C., Hong, Y. (2024). Chewing characteristics of rice and reasons for differences between three rice types with different amylose contents. *Int. J. Biol. Macromol.*, 278, 134869. doi:10.1016/j.ijbiomac.2024.134869

Miao, W., Wang, L., Xu, X., and Pan, S. (2016). Evaluation of cooked rice texture using a novel sampling technique. *Measurement*, **89**, 21–27. doi:10.1016/j.measurement.2016.03.072

Nakamura, S., Cui, J., Zhang, X., Yang, F., Xu, X., Sheng, H., and Ohtsubo, K. (2016). Comparison of eating quality and physicochemical properties between Japanese and Chinese rice cultivars. *Biosci., Biotechnol., Biochem.*, **80**, 2437–2449. doi:10.1080/09168451.2016.1220823

Nasato, D.S., Albuquerque, B.Q., and Briesen, H. (2021). Predicting the behavior of granules of complex shapes using coarse-grained particles and artificial neural networks. *Powder Technol.*, **383**, 328–335. doi:10.1016/j.powtec.2021.01.029

Pan, J., Chen, X., Zhu, Y., Xu, B., Li, C., Khin, M.N., Cui, H., and Lin, L. (2024). Design and development of dual-extruder food 3D printer based on selective compliance assembly robot arm and printing of various inks, *J. Food Eng.*, **370**, 111973. doi:10.1016/j.jfoodeng.2024.111973

Panngom, K., Penjumras, P., Panjan, W., Sornsakdanuphap, J., Suanpoot, P., Yoosuk, S., and Wattananapakasem, I. (2024). Improving the cooking quality of black glutinous rice by using the low-pressure cold plasma technology. *J. Food Sci. Technol.* doi:10.1007/s13197-024-06060-7

Tamura, M., Shinohe-Oshima, M., and Saito, T. (2024). Performance of non-waxy Japonica rice in the post-cooking storage process and with a varying water-to-rice ratio. *Appl. Food Res.*, **4**, 100366. doi:10.1016/j.afres.2023.100366

Tien, N.N.T., Phi, N.T.L., Thu, N.N.A., Oanh, T.T.H., and Hung, P.V. (2024). Cooking quality, textural characteristics and sensory evaluation of heat-moisture treated unpolished red rice under different cooking conditions. *Int. J. Food Sci. Technol.*, **59**, 7776–7785. doi:10.1111/ijfs.16913

Tong, K., Yu, F., Dai, Z., Wang, H., Huang, K., Chen, S., and Guo, J. (2024). Micro-level unloading behaviors of clay aggregates: A coarse-grained molecular dynamics study. *Powder Technol.*, **443**, 119922. doi:10.1016/j.powtec.2024.119922

Wu, X., Zhou, Y., Lu, Q., and Liu, R. (2023). Ultrasonic-assisted immersion of parboiled treatment improves head rice yield and nutrition of black rice and provides a softer texture of cooked black rice. *Ultrason. Sonochem.*, **95**, 106378. doi:10.1016/j.ultsonch.2023.106378

Xu, J., Xu, B., Zhan, H., Xie, Z., Tian, Z., Lu, Y., Wang, Z., Yue, H., and Yang, F. (2024). A soft robotic system imitating the multimodal sensory mechanism of human fingers for intelligent grasping and recognition. *Nano Energy*, **130**, 110120. doi:10.1016/j.nanoen.2024.110120

Xu, Y., Lv, B., Wu, P., and Chen, X.D. (2024). Creating similar food boluses as that in vivo using a novel in vitro bio-inspired oral mastication simulator (iBOMS-III): The cases with cooked rice and roasted peanuts. *Food Res. Int.*, **190**, 114630. doi:10.1016/j.foodres.2024.114630

Yi, X., Yu, W., Liu, H., and Li, C. (2024). Importance of both leached and residual starch molecular structures in determining cooked rice texture at different rice-to-water cooking ratios. *Int. J. Biol. Macromol.*, **258**, 129040. doi:10.1016/j.ijbiomac.2023.129040

Yin, X., Chen, X., Hu, J., Zhu, L., Zhang, H., and Hong, Y. (2023). Effects of distribution, structure and interactions of starch, protein and cell walls on textural formation of cooked rice: A review. *Int. J. Biol. Macromol.*, **253**, 127403. doi:10.1016/j.ijbiomac.2023.127403

Zhang, S., Fu, A., Guo, M., Li, J., Tan, Z., Guo, T., Zhou, H., and Yang, G. (2024). Effect and identification of different allele combinations of SSIIa and Wx on rice eating and cooking quality. *Euphytica*, **220**, 63. doi:10.1007/s10681-024-03329-y

Zhang, W., Yang, Y., Zhang, J., Zheng, W., Du, Y., and Dang, B. (2024). Study of the effect of milling on nutritional and sensory quality and volatile flavor compounds of cooked highland barley rice. *LWT-Food Sci. Technol.*, **198**, 115972. doi:10.1016/j.lwt.2024.115972

Zhang, Y., Li, F., Huang, K., Li, S., Cao, H., Xie, J., and Guan, X. (2023). Structural changes of starch under different milling degrees affect the cooking and textural properties of rice. *Food Chemistry: X*, **17**, 100627. doi:10.1016/j.fochx.2023.100627

Zheleznyakova, A.L. (2021) A cost-effective computational approach based on molecular dynamics for generating 3D packs of irregularly-shaped grains in a container of complex geometry. *Powder Technol.*, **394**, 403–423. doi:10.1016/j.powtec.2021.08.070

Zuo, Z., Zhang, M., Li, T., Zhang, X., and Wang, L. (2024). Quality control of cooked rice: Exploring physicochemical changes of the intrinsic component in production. *Food Chem.*, **463**, 141295. doi:10.1016/j.foodchem.2024.141295

URL cited

i) https://www.maff.go.jp/j/zyukyu/fbs/attach/pdf/index-26.pdf (in Japanese) (Oct 4, 2024).

ii) https://www.maff.go.jp/j/zyukyu/jki/j_doutai/attach/pdf/doutai_top-141.pdf (in Japanese) (Oct 4, 2024).